

AD-A271 863



2

FINAL REPORT

for the period

October 1, 1990 through September 30, 1992

Sponsored by
Office of Naval Research
Grant No. N00014-91-J-1245

"Nearshore Wave Processes"

Dr. Gary Griggs
Principal Investigator

DTIC
ELECTE
NOV 02 1993
S B D

DISTRIBUTION STATEMENT A
Approved for public release
Distribution Unlimited

93-26312



6/9/93

UNDERTOW IN THE SURFZONE

Abstract

Waves breaking on a beach drive a vertically sheared cross-shore flow, directed onshore near the surface and offshore near the bed. Models, based on conservation of both mass and momentum flux, exist for monochromatic waves and have been tested in laboratories. They provide predictions for the vertical profile of the mean cross-shore currents below the wave trough level which agree qualitatively well with the measurements. This study extends these models to random waves and tests them with field data. A second class of model, based on incomplete physics but valid over the whole water column, is developed and also compared with the measurements.

Data from two field experiments are used in this study to make a statistically meaningful test of the models. Three current meters over the vertical were deployed on a sled during the SuperDuck Experiment held near Duck, North Carolina during October 1986. Five current meters over the vertical were deployed at each of three stacks at Scripps Institution of Oceanography, La Jolla, California during March and April 1987.

DISC QUALITY INSPECTED 5

Accession For	
NTIS GRA&I	<input checked="" type="checkbox"/>
DTIC TAB	<input type="checkbox"/>
Unannounced	<input type="checkbox"/>
Justification	
By	<i>per letter</i>
Distribution/	
Availability Codes	
Dist	Avail and/or Special
<i>A-1</i>	

Model comparisons with the data from both field experiments show that, while the models give values that are within the expected range, they do not yet adequately predict the vertical structure of the velocity profile over the water column. The statistical measures of fit reported in this study give additional quantitative insights into the behavior of the models.

List of Figures

- Figure 1: A schematic of the cross-shore depth-averaged estimate of the mean current
- Figure 2: The Rayleigh distribution $P(H)$ and the broken wave weighting function $W(H)$
- Figure 3: A schematic of the mass model
- Figure 4: The Rayleigh distribution with all waves amplitude bigger than z selected
- Figure 5: The Rayleigh distribution with all waves with amplitude less than z selected
- Figure 6: Three model profiles and measurements from Scripps run 17ac
- Figure 7: Three typical profiles showing the variation in the shear stress as a function of v_t
- Figure 8: Map of North Carolina
- Figure 9: A simplified schematic of the SuperDuck sled
- Figure 10: A typical set of measurements and a typical beach profile during SuperDuck
- Figure 11: Plot of the SuperDuck sled data used in this study
- Figure 12: Map of Southern California
- Figure 13: A typical beach profile during the Scripps UnderTow Experiment and the location of the three fixed stacks of instruments
- Figure 14: Scripps's instrument layout during the UnderTow Experiment
- Figure 15: A schematic of an intermittently submerged current meter

- Figure 16: The location of the Scripps current meters in relative water depth versus the fraction of time they spent in the water.
- Figure 17: Scripps UnderTow data plotted on scaled axes
- Figure 18: The statistical measures of fit between the mass model and the Scripps data, graphed as a function of the parameters n and γ
- Figure 19: Scatter plots of the mass model compared with all Scripps sensors.
- Figure 20: Scatter plots of the mass model compared with Scripps meters located the wave trough
- Figure 21: Line of perfect agreement between the model and measurements
- Figure 22: Scatter plot of the fit between the wave height predictions and the Scripps measured wave heights.
- Figure 23: Typical scaled profiles predicted by the momentum model.
- Figure 24: Statistical measures of fit between the momentum model and all Scripps data located below the wave trough.
- Figure 25: Scatter plot and statistics of the comparison of the momentum with the Scripps data below trough level.
- Figure 26: Scatter plot and statistics from the comparison of the mass model with the SuperDuck data.
- Figure 27: Scatter plot and statistics from the comparison between the mass model and the SuperDuck data located below the trough level.

Figure 28: Scatter plot and statistics from the comparison between the momentum model and SuperDuck measurements located below the trough level.

Figure 29: Scatter plot and statistics from the comparison between the momentum model and the Scripps sensors located in the lower quarter of the water column.

List of Tables

- Table 1:** A list of SuperDuck sled runs used in this study
- Table 2:** A list of Scripps runs used in this study.
- Table 3:** Statistical measures of fit for the mass model - data comparisons with the Scripps UnderTow data.
- Table 4:** Summary of statistic for the comparisons between the mass model and the field data
- Table 5:** Summary of statistic for the comparisons between the momentum model and the field data
- Table 6:** Summary of statistic for the comparisons between the momentum model and the field data located in the lower quarter of the water column

Acknowledgments

This study was funded by grant N00014-91-J-4107-P00001, issued by the Office of Naval Research. The research was carried out under the supervision of Professor Gary Griggs at the University of California, Santa Cruz, Professor Ed Thornton at the Naval Postgraduate School, Monterey, and Professor Bob Guza at the University of California, San Diego. Without their generosity and special insights this project would have been more intractable, and certainly much less enjoyable.

Objectives

Undertow is an offshore directed flow below the wave trough level which, on a 2-dimensional beach, compensates for a shoreward mass transport induced by the waves above the trough-level. Undertow has been observed in the laboratory by Russel and Osorio (1956), Svendsen and Hansen (1984), Stive and Wind (1986), and Okaysu, Shibayama and Horikawa (1988), and on the natural beach by Greenwood and Osborne (1990).

Undertow may play an important role in the off-shore flow of sediment in the surfzone under large waves, and sediment transport models such as Baillard (1981) include the near-bottom mean currents as a parameter. While depth-averaged current theories are well developed, researchers have recognized that there can exist significant shear in the vertical velocity profile under breaking waves.

Two competing theories exist for the vertical structure of the mean cross-shore flow based on differing boundary conditions for the cross-shore momentum-balance; Stive et al (1986, 1987) and Svendsen et al (1984, 1987, 1988, 1989). Both models predict a general parabolic shape below the wave trough level and the results only differ significantly outside the surfzone. A simple heuristic model, dependent on only local variables, is offered as an alternative to the previous approaches. The

model is easy to implement and, while possibly lacking some important physics, it gives predictions over the whole water column.

Two sets of field measurements are used for model-data comparisons. The Naval Postgraduate School deployed a sled during the October 1986 SuperDuck experiment hosted by the U.S. Army Corps of Engineers Field Research Facility, Duck, North Carolina. The sled housed three current meters over the vertical and a pressure sensor. Twenty-one 30 minute runs were extracted from the measurements for use with this study. Scripps Institution of Oceanography deployed instruments at Torrey Pines, California during the spring of 1987. Three stacks, each consisting of five current meters over the vertical and two pressure sensors, were located along a cross-shore transect. Approximately eighty 1 hour runs were extracted for use in this study.

This thesis compares the models for undertow with the measurements and provides five statistical measures to serve as a basis for interpreting the results. This is a quantitative comparison of the theories to data where previously researchers have presented only qualitative comparisons.

Models for Mean Cross-Shore Currents

Two categories of models are developed for comparison with the field data. In the ensuing discussion the variable x represents the cross-shore direction, u represents the cross-shore flow, positive offshore, and z the vertical direction, referenced from the mean water line and positive upward, and w the vertical velocity. Time averaging will be represented with an horizontal overbar and ensemble averaging with the angle brackets.

Mass Transport Due to Monochromatic Waves

Common to all the models is the two-dimensional assumption that, on average, as much water moves on-shore as moves off-shore. How much water is that? Depth averaged theory gives us an estimate for either the mean shoreward flow in the wave layer, U_f , or the return flow in the lower water column, U_r . It forms the basis for all of the models and, since we will need estimates of U_r , we present the concepts and a derivations of the commonly used forms. The game plan is to start with monochromatic non-breaking wave theory, (Phillips, 1977), add

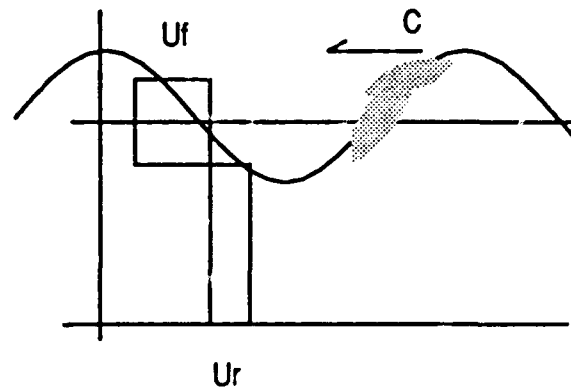


Figure 1: A schematic of the cross-shore depth-averaged estimate of the mean current.

a simple breaking wave model (Stive and Wind, 1982), and extend it to random wave theory, (Thornton and Guza, 1983).

The net cross-shore mass flux, M_f , in the direction of wave travel in an Eulerian reference is integrated over the wave surface from trough to crest.

$$M_f = \overline{\int_0^n \rho u(z) dz} \quad (1)$$

For non-breaking monochromatic waves, Phillips, (1977), approximated the wave velocity in the crest-trough region using a Taylor Series expansion. To lowest order $u(z)$ is approximated as uniform between crest and trough and,

$$M_f = \frac{\rho g H^2}{8 C} \quad (2)$$

It follows that, in shallow water, the depth-averaged shoreward-directed mean flow in the wave trough to crest region U_f is

$$U_f = \frac{M_f}{\rho H} = \frac{g H}{8 C} = \frac{1}{8} \sqrt{\frac{g}{h}} H \quad (3)$$

and is assumed uniform over the vertical. Since we require that the return flow balance with the shoreward flow it follows that,

$$U_r = - \frac{1}{8} \sqrt{\frac{g}{h}} \frac{H^2}{d_t} \quad (4)$$

Under breaking waves there is an additional contribution to the net mean shoreward flow which is modeled as a plug of water, known as the

roller, that moves approximately with the wave propagation speed C . An empirically derived expression was presented in Stive and Wind (1982) for monochromatic breaking waves in shallow water,

$$U_r d_t = -U_f H = -\int_{\eta_t}^{\eta_c} u dz \approx -\frac{1}{10} \sqrt{\frac{g}{h}} H d_t \quad (5)$$

where η_c is the wave crest level. Then,

$$U_f = \frac{1}{10} \sqrt{\frac{g}{h}} d_t \quad (6)$$

$$U_r = -\frac{1}{10} \sqrt{\frac{g}{h}} H \quad (7)$$

Another model for the roller contribution is by Svendsen (1984) in which the mass flux per unit wave length supplied by the roller is given by

$$M_R = \rho \frac{AC}{L} = \rho \frac{A}{T} \quad (8)$$

where L is the wave length and T the time period. Svendsen, (1984) estimates the area $A = 0.9 H^2$. In this case, the total mass transport is found by adding the roller contribution to the unbroken result.

Extension to Random Breaking Waves

The monochromatic case is extended to random waves following work by Thornton and Guza (1983). It is assumed the wave height

distribution at any location, either outside or inside the surf zone, is well described by the Rayleigh distribution.

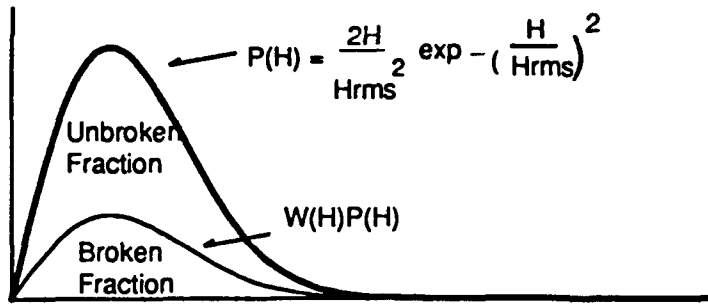


Figure 2: The Rayleigh distribution $P(H)$ and the broken wave weighting function $W(H)$.

At any depth a percentage of the waves are breaking, which is assumed to be a weighted fraction of the Rayleigh distribution,

$P_b(H) = W(H) P(H)$, where $W(H)$ is a weighting function. Thornton and Guza (1983) gave a simple form for $W(H)$ which is dependent not on H but on H_{rms} , γ and h .

$$W(H) = \left(\frac{H_{rms}}{\gamma h} \right)^n \quad (9)$$

where n is determined from the measurements. The unbroken fraction of waves is given by

$$P_u(H) = P(H) [1 - W(H)] \quad (10)$$

An expression for the net depth-averaged return flow in the upper layer, $\langle U_f \rangle$ is obtained by estimating the contributions from the unbroken

waves, $\langle U_{uf} \rangle$, and the broken waves $\langle U_{bf} \rangle$, such that, $\langle U_f \rangle = \langle U_{uf} \rangle + \langle U_{bf} \rangle$.

Then, applying equations 6 and 10,

$$\langle U_{uf} \rangle = \int_0^\infty U_{uf} P_u(H) dH = \frac{\sqrt{\pi}}{16} \sqrt{\frac{g}{h}} \left[1 - \left(\frac{H_{rms}}{\gamma h} \right)^n \right] H_{rms} \quad (11)$$

and, using equation 8,

$$\langle U_{bf} \rangle = \int_0^\infty U_{br} P_b(H) dH = \frac{1}{10} \sqrt{\frac{g}{h}} \left(\frac{H_{rms}}{\gamma h} \right)^n \left[h - \frac{\sqrt{\pi}}{4} H_{rms} \right] \quad (12)$$

Likewise, expressions for the depth-averaged return flow below the trough level from the unbroken waves, $\langle U_{ur} \rangle$, and broken waves, $\langle U_{br} \rangle$, are found by applying equations 4 and 7 and retaining terms to order H ,

$$\langle U_{ur} \rangle = \int_0^\infty U_{ur} P_u(H) dH = \frac{1}{8h} \sqrt{\frac{g}{h}} \left[1 - \left(\frac{H_{rms}}{\gamma h} \right)^n \right] H_{rms}^2 \left[1 + \frac{3\sqrt{\pi}}{8} \frac{H_{rms}}{h} \right] \quad (13)$$

$$\langle U_{br} \rangle = \int_0^\infty U_{br} P_b(H) dH = -\frac{\sqrt{\pi}}{20} \sqrt{\frac{g}{h}} \left(\frac{H_{rms}}{\gamma h} \right)^n H_{rms} \quad (14)$$

Mass Balance Model

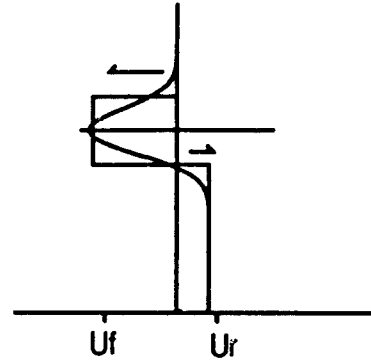


Figure 3: A schematic of the mass model

The simplest model is based on the conservation of mass-flux and approximates the return flow as uniform over the vertical and equal to the onshore transport. This model has the advantage of requiring only local knowledge of wave height and water depth and it predicts a velocity profile over the entire water column. In the extension to random waves the expressions for the depth-averaged mean currents for monochromatic waves are used for each wave height. At each level z the flow is partitioned into the contributions from breaking and non-breaking waves and averaged over the appropriate portion of the Rayleigh distribution.

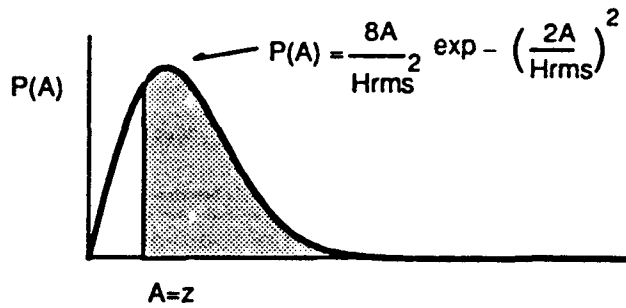


Figure 4: The Rayleigh distribution with all waves with amplitude bigger than z selected.

In the upper wave layer, at any elevation z above the mean water line, only waves with amplitude at least as big as z can add to the mean flow there. Smaller waves have no affect. The contribution from the unbroken waves is found by utilizing equation 3

$$\begin{aligned} \langle u_{uf}(z) \rangle &= \int_{A=z}^{\infty} u_{uf}(z) P_u(A) dA \\ &= \frac{1}{4} \sqrt{\frac{g}{h}} H_{rms} \left[1 - \left(\frac{H_{rms}}{\gamma h} \right)^n \right] \left[S \exp(-S^2) + \frac{\sqrt{\pi}}{2} \text{erfc}(S) \right] \end{aligned} \quad (15)$$

$$\text{where } S = \left(\frac{2z}{H_{rms}} \right)$$

The contribution from the broken waves is found by integrating equation 6

$$\begin{aligned} \langle u_{bf}(z) \rangle &= \int_{A=z}^{\infty} U_{bf} P_b(A) dA \\ &= \frac{1}{10} \sqrt{\frac{g}{h}} \left(\frac{H_{rms}}{\gamma h} \right)^n \left[(h-z) \exp(-S^2) - \frac{\sqrt{\pi}}{4} H_{rms} \text{erfc}(S) \right] \end{aligned} \quad (16)$$

These equations are valid for $z > 0$. Since the wave layer extends to the trough level and is symmetrical about the mean water line, reflect these equations about $z = 0$ for the complete solution in the wave layer.

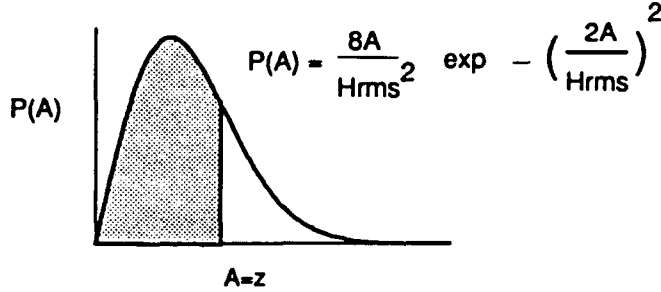


Figure 5: Rayleigh distribution with all waves with amplitude less than z selected

Approximate the return flow below the mean water line where only waves with an amplitude smaller than z can contribute. Larger waves depress the trough level below z . The contribution from the unbroken waves is found utilizing equation 4

$$\begin{aligned} \langle u_{ur}(z) \rangle &= \int_0^{A=z} U_{ur} P_u(A) dA \\ &= \frac{1}{8} \sqrt{\frac{g}{h}} H_{rms}^2 \left[1 - \left(\frac{H_{rms}}{\gamma h} \right)^n \right] \left[(T^2 + 1) \exp(-T^2) - 1 \right] \\ &\quad + \frac{H_{rms}}{2h} \left[\left\{ T^2 + \frac{3}{2} \right\} T \exp(-T^2) - \frac{3\sqrt{\pi}}{4} \text{erf}(T) \right] \end{aligned} \quad (17)$$

$$\text{where } T = \left(\frac{2|z|}{H_{rms}} \right)$$

The contribution from the broken waves is found using equation 7

$$\begin{aligned} \langle u_{br}(z) \rangle &= \int_0^{A=\infty} U_{br} P_b(A) dA \\ &= \frac{1}{10} \sqrt{\frac{g}{h}} H_{rms} \left(\frac{H_{rms}}{\gamma h} \right)^n \left[T \exp(-T^2) - \frac{\sqrt{\pi}}{2} \text{erf}(T) \right] \end{aligned} \quad (18)$$

Adding the solution for the top and the bottom together provides the vertical profile. Typical profiles are shown in Figure 6. A typical model profile is given in figure 6 plotted alongside measurements.

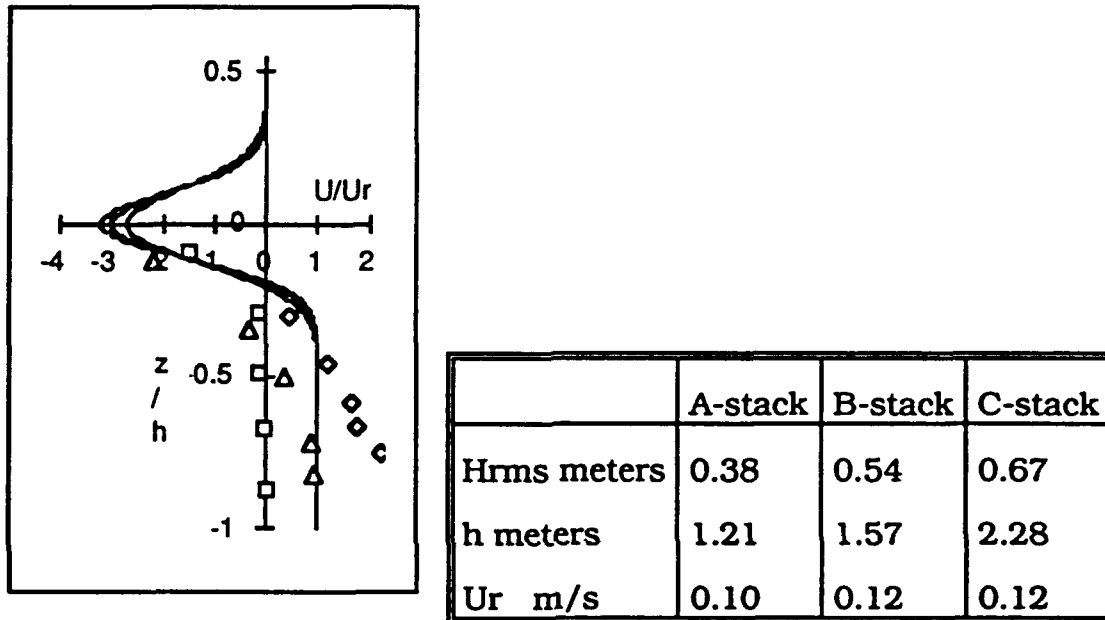


Figure 6: Three model profiles and measurements from Scripps run17ac. The 3 lines are the predictions at the three stacks, which appear almost equal on this scaled plot. The diamond markers are the measurements: are from the C-stack, the squares are from the B-stack and the triangles are from the A-stack. The scaling parameters are given in the table.

The Momentum Model

Two models by Stive and Wind (1986) and Uday and Svendsen (1993) are developed below. The models are formulated in a similar manner differing only by their choice of boundary conditions. The model by Stive and Wind is described first.

Models based on the conservation of momentum across the surfzone provide a more realistic description of the physics and predict a sheared profile for the return flow. Mass balance is still a requirement in this model and is used as a boundary condition to resolve an integration constant. The theory rests upon the cross-shore and vertical Navier Stokes momentum equations. The velocities are partitioned into their mean \bar{u} , wave \bar{u} , and turbulent u' , contributions and time averaged. The vertical momentum equation for the pressure is solved and combined with the cross-shore momentum equation. Assuming isotropic turbulence and steady 2-D flow, Stive and Wind, (1986) show

$$-\frac{\partial}{\partial z}\rho(\overline{u'w'}) = g\frac{\partial\rho\bar{\eta}}{\partial x} + \frac{\partial}{\partial x}\rho(\overline{u^2} - \overline{w^2}) + \frac{\partial}{\partial z}\rho(\overline{uw}) \quad (19)$$

where

- $\bar{\eta}(x)$ is the mean surface elevation known as wave setup
- g is the acceleration due to gravity
- ρ is the water density

The turbulent Reynolds stress is modeled using an eddy-viscosity formulation

$$\tau(z) = -\rho(\overline{u'w'}) = \rho v_t \frac{\partial \bar{u}}{\partial z} \quad (20)$$

where v_t is the eddy viscosity coefficient. The last term in equation 19 can be simplified if the wave motion is irrotational.

$$\frac{\partial \bar{u}}{\partial z} = \frac{\partial \bar{w}}{\partial x} \quad (21)$$

This assumption is good outside the surfzone. Even inside the surfzone, the turbulence of the breaking waves is primarily confined to the crest-trough region and this approximation appears to be reasonable (see Thornton, (1979)). Using the continuity equation,

$$\frac{\partial \bar{u}}{\partial x} = -\frac{\partial \bar{w}}{\partial z} \quad (22)$$

then

$$\frac{\partial}{\partial z}(\overline{u'w'}) = \overline{u \frac{\partial w'}{\partial z}} + \overline{w' \frac{\partial u}{\partial z}} = -\overline{u \frac{\partial u}{\partial x}} + \overline{w' \frac{\partial w'}{\partial x}} = -\frac{1}{2} \frac{\partial}{\partial x}(\overline{u^2} - \overline{w^2}) \quad (23)$$

Substituting equations 20 and 23 into equation 19 gives

$$\frac{\partial}{\partial z} \tau(z) = \frac{\partial}{\partial z} \rho v_t \frac{\partial}{\partial z} \bar{u}(z) = \frac{\partial R}{\partial x} \quad (24)$$

$$\text{where the wave forcing term } R = \rho \left[\frac{1}{2} (\overline{u^2} - \overline{w^2}) + g\eta \right] \quad (25)$$

This method for deriving the wave forcing, while different from Svendsen's method in the details, gives the same net result. Stive and Wind's R differs because they assume that the oscillating contribution to

stress is small compared with the Reynolds stress, $\rho(\overline{u\overline{w}}) \ll \rho(\overline{u\overline{w}})$ hence they use $R = \rho(g\overline{\eta} + \overline{u^2} - \overline{w^2})$. We will use equation 25.

If R is constant over depth, equation 24 can be integrated to yield the shear stress. Stive and Wind (1986) gave empirical evidence from laboratory studies to indicate R is constant over the vertical and they assumed so. However, it is easy to show R constant over the vertical, even in intermediate water depth, using linear theory and substituting the wave velocities \overline{u} and \overline{w} and averaging in time. In shallow water linear theory directly predicts wave orbital velocities which do not vary with depth. Integrating equation 24,

$$\rho v_t \frac{\partial}{\partial z} \overline{u}(z) = \tau(z) = \frac{\partial R}{\partial x} z + C_1 \quad (26)$$

Integrating a second time,

$$\overline{u}(z) = \frac{1}{2\rho v_t} \frac{\partial R}{\partial x} z^2 + \frac{1}{\rho v_t} C_1 z + C_0 \quad (27)$$

Stive and Wind, (1986), obtained C_1 by integrating equation 24 from the trough level η_t , to the sea-bed $-h$, and solved for the shear stress at the trough level.

$$\overline{\tau}(\eta_t) = \frac{\partial R(x)}{\partial x} d_t + \overline{\tau}_b \quad (28)$$

where $d_t = \eta_t + h$ is the depth below trough level, and $\overline{\tau}_b$ is the shear stress at the seabed. Using this result, equation 26 is evaluated at the trough level to solve for C_1

$$C_1 = \frac{\partial R(x)}{\partial x} h + \bar{\tau}_b \quad (29)$$

For completeness, the shear stress at any depth z is given by

$$\bar{\tau}(z) = \frac{\partial R}{\partial x} (z+h) + \bar{\tau}_b \quad (30)$$

C_0 is resolved by using the conservation of mass criteria that the amount of water traveling shoreward above the wave trough level M_r , is balanced by an equal amount of water traveling offshore in the lower part of the water column M_r , such that $M_r = -M_r$. The depth-averaged mean return flow U_r is defined by $M_r = U_r d_t$. Stive and Wind (1986) applied this below trough level,

$$\int_{-d_t}^{\eta_t} \bar{u}(z) dz = U_r d_t \quad (31)$$

This evaluates to

$$C_0 = U_r - \frac{1}{6\rho v_t} \frac{\partial R}{\partial x} \frac{1}{d_t} \{ \eta_t^3 + 3\eta_t^2 h - 2h^3 \} - \frac{1}{2\rho v_t} \bar{\tau}_b (\eta_t - h) \quad (32)$$

Substituting equations 29 and 32,

$$\bar{u}(z) = \frac{1}{2\rho v_t} \frac{\partial R}{\partial x} z^2 + \frac{1}{\rho v_t} \frac{\partial R}{\partial x} hz + \frac{1}{6\rho v_t} \frac{\partial R}{\partial x} \{ 3h^2 - d_t^2 \} + \frac{\bar{\tau}_b}{\rho v_t} \left\{ z+h - \frac{d_t}{2} \right\} + U_r \quad (33)$$

Setting $\xi = (z+h)/d_t$. Stive and Wind's (1986) form can be derived

$$\bar{u}(z) = \frac{1}{2} \left[(\xi-1)^2 - \frac{1}{3} \right] \frac{d_t^2}{\rho v_t} \frac{\partial R}{\partial x} + \left(\xi - \frac{1}{2} \right) \frac{d_t \bar{\tau}_b}{\rho v_t} + U_r \quad (34)$$

Following the derivation of Svendsen et al (1987), Svendsen and Hansen (1988), and Uday and Svendsen (1993), the integration constant C_1 is solved by defining a thin but significant bottom boundary layer which is matched to the solution at the top of this boundary. The bottom boundary has a thickness δ and the top of the bottom boundary layer is located at $z_b = -h + \delta$. Above the bottom boundary layer, and below the trough level, the water motions are defined by equations 1 through 25. In the bottom boundary layer,

$$\frac{\partial}{\partial z} \rho v_b \frac{\partial \bar{u}}{\partial z} = \frac{\partial}{\partial z} \rho (\overline{u'w'}) = \frac{\partial}{\partial z} \rho \eta + \frac{\partial}{\partial x} \rho (\bar{u}^2 - \bar{w}^2) + \frac{\partial}{\partial z} \rho (\bar{u}\bar{w}) \quad (35)$$

where v_b is the eddy viscosity coefficient in the bottom boundary layer and is distinctly different from the coefficient v_t in the middle layer. Matching the shear stresses at the top of the bottom boundary layer,

$$\rho v_b \frac{\partial \bar{u}}{\partial z} \Big|_{z_b} = \rho v_t \frac{\partial \bar{u}}{\partial z} \Big|_{z_b} = \tau_b \quad (36)$$

Integrating equation 35 from the seabed to the top of the boundary layer

$$\rho v_b \frac{\partial \bar{u}}{\partial z} \Big|_{z_b} - \rho v_b \frac{\partial \bar{u}}{\partial z} \Big|_{z_a} = \int_{z_a}^{z_b} \left[\frac{\partial}{\partial z} \rho \eta + \frac{\partial}{\partial x} \rho (\bar{u}^2 - \bar{w}^2) \right] dz + \rho (\bar{u}\bar{w}) \Big|_{z_b} - \rho (\bar{u}\bar{w}) \Big|_{z_a} \quad (37)$$

Where

$$\tau_s = -\rho(\bar{u}\bar{w}) \Big|_{z_b} \quad (38)$$

is the stress due to the steady streaming velocity at the top of the bottom boundary layer. Svendsen (1984), and Uday and Svendsen (1993) assume that the wave forcing is small in the boundary layer,

$$\int_{-1}^{z_b} \left[\frac{\partial}{\partial z} \rho \pi + \frac{\partial}{\partial x} \rho (\bar{u}^2 - \bar{w}^2) \right] dz = 0 \quad (39)$$

and requiring a no slip condition at the seabed then the wave stress vanishes there

$$\rho(\bar{u}\bar{w}) \Big|_{-1} = 0 \quad (40)$$

then, equation 37 simplifies to

$$\tau_{z_b} = \rho v_b \frac{\partial \bar{u}}{\partial z} \Big|_{z_b} = \tau_b - \tau_s \quad (41)$$

C_1 is found by applying equation 26 at the top of the bottom boundary layer

$$C_1 = \tau(z_b) - \frac{\partial R}{\partial x} z_b = \tau_b - \tau_s - \frac{\partial R}{\partial x} z_b \quad (42)$$

and the expression for the shear stress becomes

$$\tau(z) = \frac{\partial R}{\partial x} (z - z_b) + \tau_b - \tau_s \quad (43)$$

C_0 is given by equation 14 and $\bar{u}(z)$ becomes

$$\bar{u}(z) = \frac{1}{2\rho v_i} \frac{\partial R}{\partial x} z^2 - \frac{1}{\rho v_i} \frac{\partial R}{\partial x} z_b z + \frac{1}{6\rho v_i} \frac{\partial R}{\partial x} (3h^2 - d_i^2) + \frac{(\tau_b - \tau_s)}{\rho v_i} \left\{ z + h - \frac{d_i}{2} \right\} + U_r \quad (44)$$

The only difference between the solutions of Svendsen and Uday (1993) and Stive and Wind (1986) is the explicit bottom boundary layer. If the boundary is thin and the stress due to the steady streaming is small then $z_b = -h$, and $\tau_s = 0$. Then equation 44 collapses to equation 33.

What is the significance of the steady streaming stress on the solution? Svendsen and Hansen (1984) say it has little influence inside the surfzone but outside Uday and Svendsen (1993) have shown it can be important in determining the vertical structure of $u(z)$

Extending the Results to Random Waves

The monochromatic description by Stive and Wind (1986) is extended to random waves by ensemble averaging over the wave distribution.

The monochromatic result expressed by equation 44 is a polynomial in z with coefficients C_2 , C_1 , and C_0 . Ensemble averaging over the wave distribution,

$$\langle \bar{u}(z) \rangle = (C_2 z^2 + C_1 z + C_0) = \int_0^\infty (C_2 z^2 + C_1 z + C_0) P(H) dH \quad (45)$$

What factors affect the shape of the profile? The curvature is a function of C_2 and C_1 , which are functions of $\frac{dR}{dx}$, calculated from wave quantities, and ν_t , a tunable parameter. Big values of $\frac{dR}{dx}$ will produce more shear than small values, while the inverse is true for ν_t . Typical momentum model profiles are shown in Figure 7 for 3 values of ν_t .

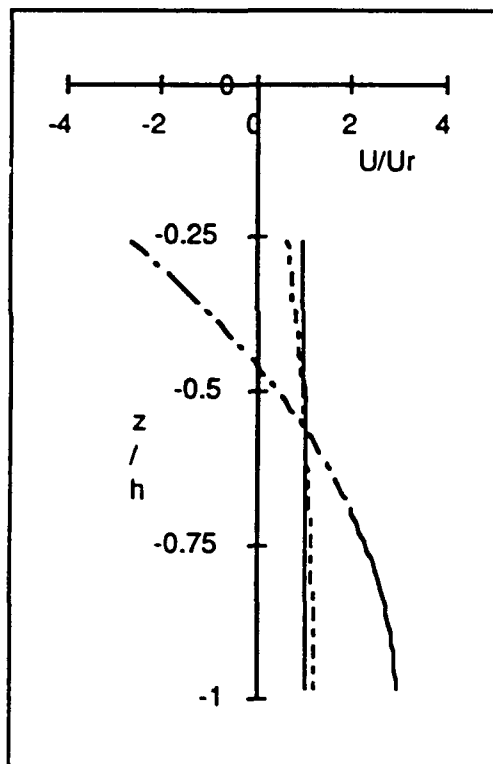


Figure 7: Three typical profiles showing the variation in the shear of the profile as a function ν_t . All other parameters being equal, the nearly vertical profile has the largest value, in this case $\nu_t = 0.1Ch$, while the strongly sheared profile has the smallest value $\nu_t = 0.001Ch$.

Wave Height Decay and Models of Wave Forcing

The wave forcing of the undertow is described by the $\frac{dR}{dx}$ term. To describe this term the wave height and the wave induced velocities are first described across the surfzone. The gradient of the wave setup, $\frac{\partial\eta}{\partial x}$, is derived from across the radiation stress momentum equation

The wave height transformation across the surfzone is modeled following Thornton and Guza (1983) in which the energy flux is balanced by the dissipation due to turbulent decay $\langle\epsilon_b\rangle$ due to wave breaking and the dissipation due to bottom friction $\langle\epsilon_f\rangle$.

$$\frac{dE C_x}{dx} = \langle\epsilon_b\rangle + \langle\epsilon_f\rangle \quad (46)$$

$\langle\epsilon_f\rangle$ is presumed small and ignored in this model. The average rate of dissipation due to wave breaking is modeled as a turbulent bore after Stoker (1956) and Hwang and Divoky (1970). Thornton and Guza (1983) extended this to the random wave model using the Rayleigh distribution for wave heights. The turbulent dissipation $\langle\epsilon_b\rangle$, is due to the breaking wave portion of the total distribution and is found by applying the symmetrical weighting function,

$$\langle\epsilon_b\rangle = \frac{3\sqrt{\pi}}{16} \rho g B^3 \bar{f} \left(\frac{H_{rms}}{\gamma h} \right)^n H_{rms}^3 \quad (47)$$

An approximation for H_{rms} is found by substituting expressions from linear theory for E and C into equation 46 and integrating shoreward from a location where the initial parameters are known.

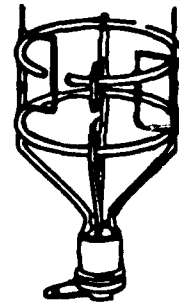
The cross-shore gradient of the wave forcing term, R , is computed at the same time as the wave height. The velocity terms are taken directly from linear theory. The wave setup is solved from the cross-shore momentum equation integrated over depth and time averaged. (see Phillips, 1977).

$$\frac{\partial \eta}{\partial x} = \frac{1}{\rho g D} \frac{\partial S_{xx}}{\partial x} \quad (48)$$

where S_{xx} is the radiation stress and D is the total water depth including wave setup. Using linear theory, the radiation stress, wave setup, and its cross-shore gradient are numerically estimated at the same time as computing the wave heights.

The Field Experiments

"Sometimes you can observe a lot by looking"
Yogi Berra



Openframe Current Meter

Two sets of field measurements are used in this study for the model-data comparisons. Data was acquired at the SuperDuck Experiment in 1986 and the Scripps UnderTow Experiment in 1987. The nearshore morphology and wave climate were significantly different at the two experiments. The SuperDuck experiment took place on a barred beach with a typical peak wave period of approximately 6 seconds. The tides at Duck are on the order of 1 meter. The Scripps experiment was located on a planar beach with a peak wave period of approximately 12 seconds and a tidal range on the order of 2 meters. The largest currents measured at both experiments were on the order of plus or minus 40 cm/sec.

The SuperDuck Experiment

The SuperDuck experiment was held at the US Army Corps of Engineers Field Research Facility (FRF) at Duck, North Carolina during the month of October 1986. The shoreline is relatively straight with the profile characterized by 1:10 sloping foreshore, a single bar and a mean slope of 1:100 offshore of the bar. The current measurements were made using Marsh-McBirney bi-directional electromagnetic current meters mounted on a movable sled. A para-scientific pressure sensor was located at the center of the sled to measure wave height, sea-surface elevation and the mean water depth. The bathymetry was measured daily during the experiment. The three current meters were mounted at elevations 0.7, 1.0 and 1.5 meters above the seabed.

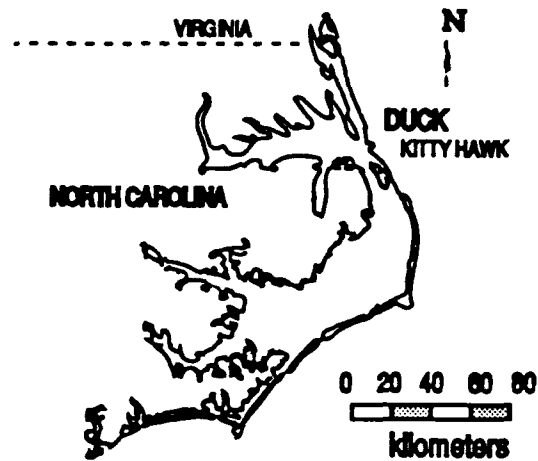


Figure 8: Map of North Carolina

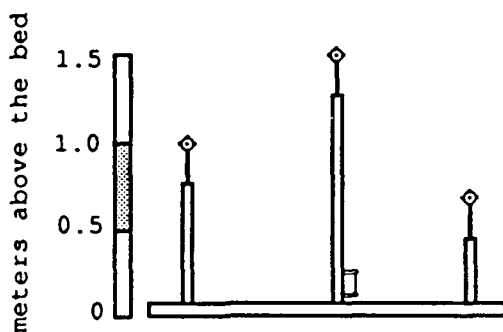


Figure 9: A simplified schematic of the SuperDuck sled

The sled was deployed by towing it offshore to the outside of the bar and pulled onshore to the measurement sites. Measurements were made just outside the bar crest, on the bar crest, inside the bar crest, and in the trough. The sled position was surveyed at the beginning and end of each run. At each location the currents were measured for at least 35 minutes. The measurements were conducted within 1-2 hours before and after high tide in order to minimize tidal height variation. The data was sampled at 8 Hz and telemetered back to shore where it was recorded.

The orientation of the current meter components relative to the alongshore bottom contours was precisely determined which was critical to the determination of the cross-shore flow direction. The alongshore contour orientation was determined by averaging the contours over 150 meters alongshore on the outer bar where the contours were reasonably linear. (See Whitford and Thornton, in press). The sled orientation was determined within ± 0.5 degrees by using an electronic surveying system to triangulate on two reflective prisms mounted 7 m up the mast of the sled on a spreader, separated by 2.4 meters. Given the sled orientation relative to the contours, and the orientation of the current meter relative to the sled, the current meters were numerically rotated in post-analysis to obtain the cross-shore and alongshore velocity components.

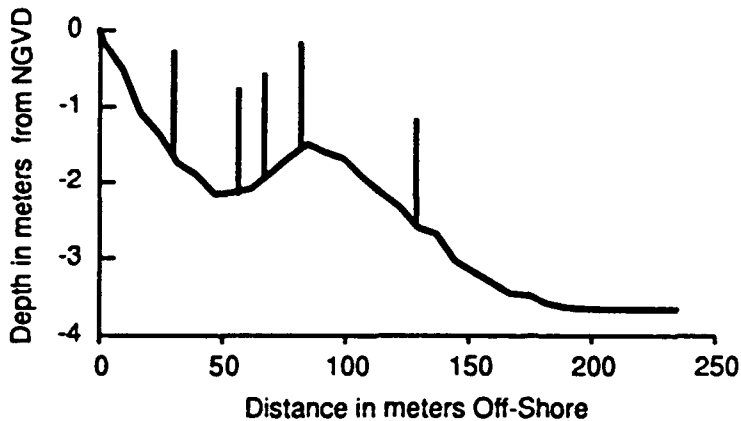


Figure 10: A typical set of measurements and a typical beach profile during SuperDuck

The SuperDuck runs used in this study are listed in Table 1. Each run was a series of collections with the most seaward given a starting index, (usually 1), which incremented for subsequent collections. The measurements used in this study are plotted in Figure 11.

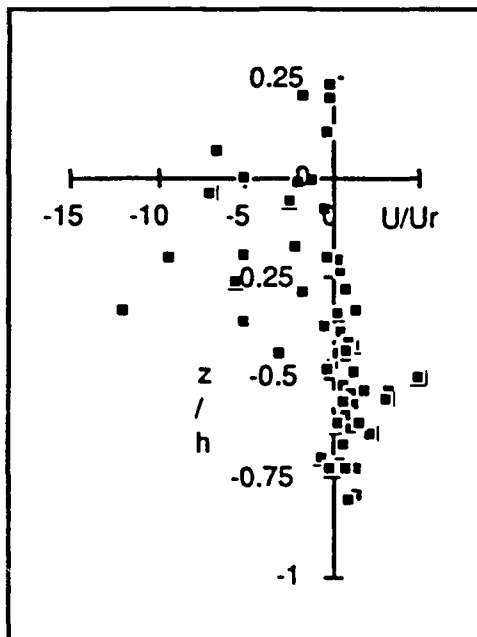


Figure 11: A plot of the SuperDuck sled data used in this study. The velocities are scaled by the theoretical depth-averaged velocity U_r , the vertical axis is scaled by the mean water depth. Twenty-one runs of 30-minute averages from SuperDuck are used in this study.

run	xloc (meters)	Hrms (meters)	peak frequency
15-1	136.010	0.92	0.16
15-2	108.010	0.76	0.16
15-3	83.510	0.57	0.16
15-4	39.010	0.59	0.16
16-2	143.700	0.98	0.19
16-3	93.200	0.80	0.19
16-4	75.200	0.57	0.19
16-5	62.200	0.52	0.19
16-6	29.200	0.49	0.19
17-1	140.700	0.72	0.19
17-2	106.200	0.69	0.19
17-3	79.200	0.57	0.19
17-4	69.700	0.41	0.19
17-5	65.700	0.36	0.19
17-6	34.200	0.24	0.19
17-7	29.200	0.26	0.19
18-1	151.700	0.93	0.19
18-2	103.200	0.84	0.19
18-3	84.700	0.67	0.19
18-4	63.200	0.38	0.19
18-5	35.200	0.28	0.19

Table 1: SuperDuck sled runs used in this study. The cross-shore positions of each run and the local measured wave heights and peak frequencies are included.

The Scripps Undertow Experiment

Bob Guza and his team from Scripps Institution of Oceanography, deployed stacks of current meters at three cross-shore locations near La Jolla, California and collected data over the course of nine days during April and March 1987. Each stack consisted of five electromagnetic current meters and two pressure gauges.

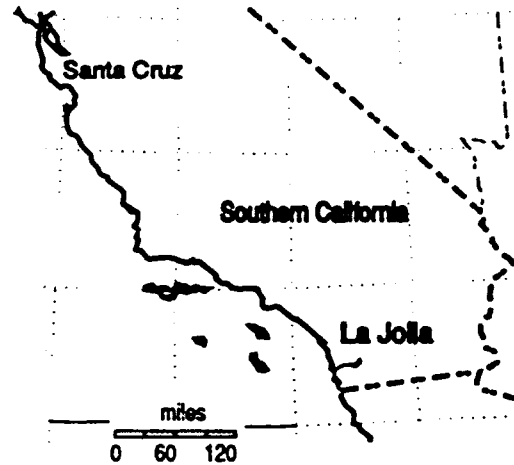


Figure 12: Map of Southern California

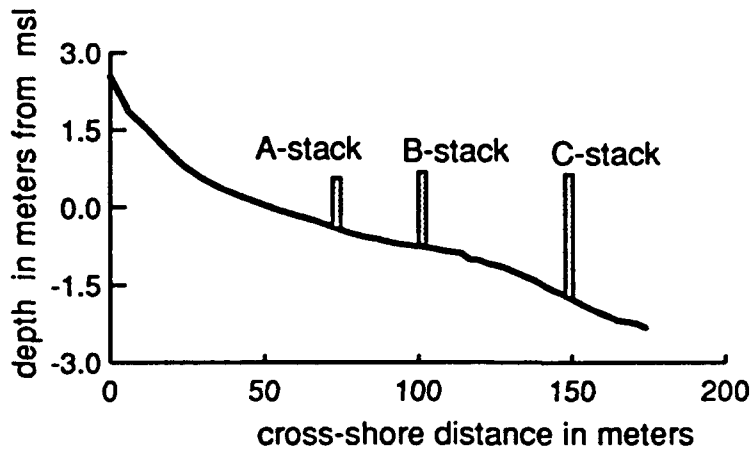


Figure 13: A typical beach profile during the Scripps UnderTow Experiment and the location of the three fixed stacks of instruments.

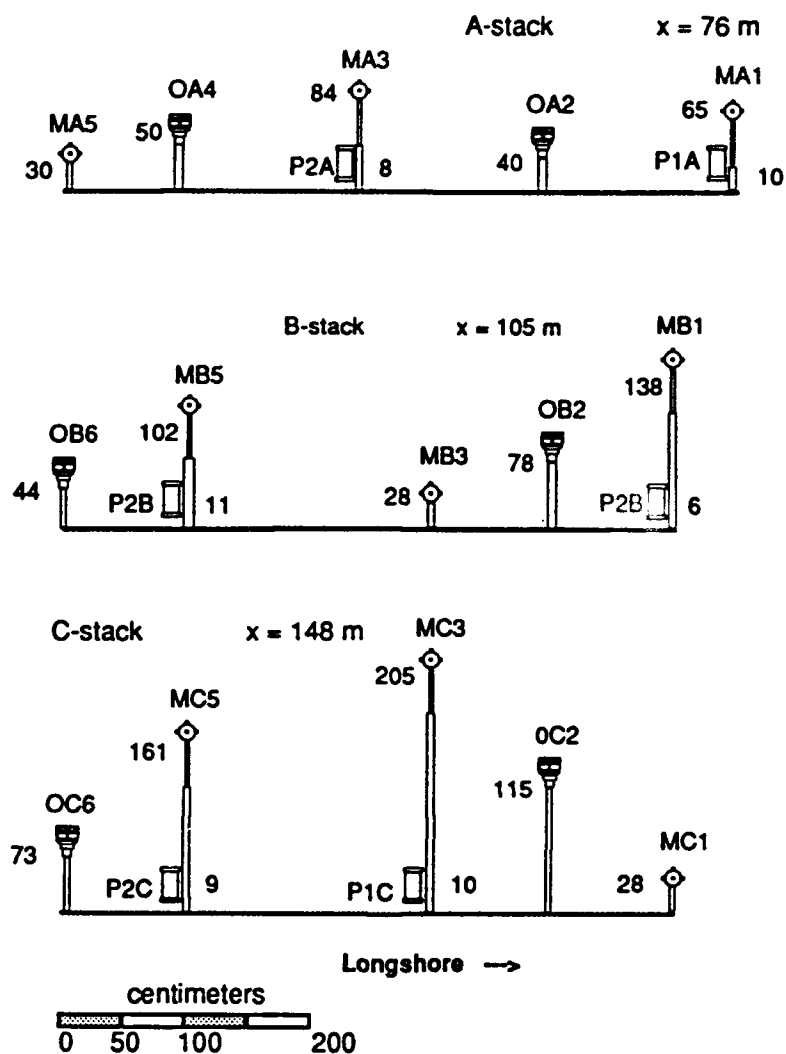


Figure 14: Scripps instrument layout during the UnderTow experiment.

Two sorts of flowmeters were deployed, the Marsh McBirney sphere design and the Scripps open-frame design. Guza-et al., (1988), compared the two sensor types and showed that they have similar characteristics. However, since the open-frame sensor is more sensitive to both the upper sea-surface and the lower bottom boundary care was taken to place those meters in the middle of the water column. The

instruments were wired into a common data acquisition system and sampled at 2 Hz. The length of the runs varied from 4 to 12.5 hours and a total of 79.8 hours of useful data were extracted for use with this study.

run	start (hour)	stop (hour)	length (hours)	date	time	hsig (cm)
3	0.4	12.6	12.2	Mar 26 1987	1824	75.0
5	24.6	37.4	12.8	Mar 27 1987	1835	59.0
6	37.7	41.7	4	Mar 28 1987	0740	47.0
7	48.6	61.3	12.7	Mar 28 1987	1834	48.0
8	61.5	66.3	4.8	Mar 29 1987	0728	41.0
9	72.9	85.9	13	Mar 29 1987	1855	28.0
10	86.1	90.6	4.5	Mar 30 1987	0805	30.0
11	96.5	109.4	12.9	Mar 30 1987	1830	33.0
12	109.5	116.0	6.5	Mar 31 1987	0730	34.0
13	120.5	133.2	12.7	Mar 31 1987	1830	36.0
17	168.0	180.4	12.4	Apr 02 1987	1800	105.0
18	183.7	191.5	7.8	Apr 03 1987	0940	186.0
19	191.5	204.2	12.7	Apr 03 1987	1732	177.0

Table 2: A List of Scripps runs used in this study. Included are the start and stop hours from epoch, length of run, date and offshore wave heights. Each run was split into 1.1 hour segments, designating the first segment as *aa*, the second *ab*, and so forth.

Field Data Analysis

The data required a significant amount of processing to get from the original input to the final mean values used in this study. A meticulous attention to detail was imperative for clean consistent results. The original calibrations were applied and a quality check was made of all the sensors. The time series was examined for inconsistencies in the means and standard deviations and the gain of one of the pressure sensors was altered, to compensate for a presumably faulty data acquisition amplifier. Each run was divided into 1.1 hour segments (8192 samples). The pressure signals were used to infer the mean water depth, the local wave height and the sea-surface signal.

Zeroing the Current Meters

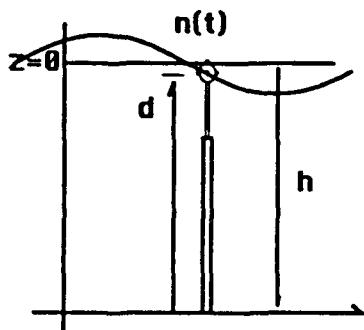


Figure 15: Schematic of an intermittently submerged current meter. Used for predicting when the meters electronically ring based on the location of the meter, d , the measured mean water depth, h , and the time series of the sea surface elevation, $n(t)$.

The current meters sitting high in the water column were intermittently submerged and a process called "zeroing the current meters" was performed on the time-series to remove the electronic ringing which corrupted the signal. By monitoring the the sea-surface signals and accounting for the mean water depth and the location of the current meter in the vertical, we deduced when the current meters were in the water. We required that the Marsh McBirney current meters be covered by at least 5 centimeters of water and the open-frame meters by at least 15 centimeters. The corresponding value in the current meter time series was set to zero if this criteria was not met.

The ratio of the total number of sample points versus the number of points not zeroed is plotted in Figure 16. This demonstrates how current meters can be relatively low in the water column and, apparently, still be coming in and out of the water. We found that the zeroing statistics of the inshore openframe current meters were the most sensitive to low wave heights and surfbeat due in a large part to our conservative requirements for being submerged 15 centimeters. For the momentum model comparisons, only data below trough is used.

Figure 16 shows that there is more than one way to choose the wave trough level for random waves. At least for this zeroing technique, trough level based on a relative water depth, such as the Hrms trough level, may include points which are only intermittently submerged. A better criteria is the fraction of time spent in the water. That is, we can

label a meter "below trough level" if the meter was reported submerged 95% of the time. We have this information for the Scripps UnderTow data but not for the SuperDuck data. For the Duck data we choose the 2Hrms trough level.

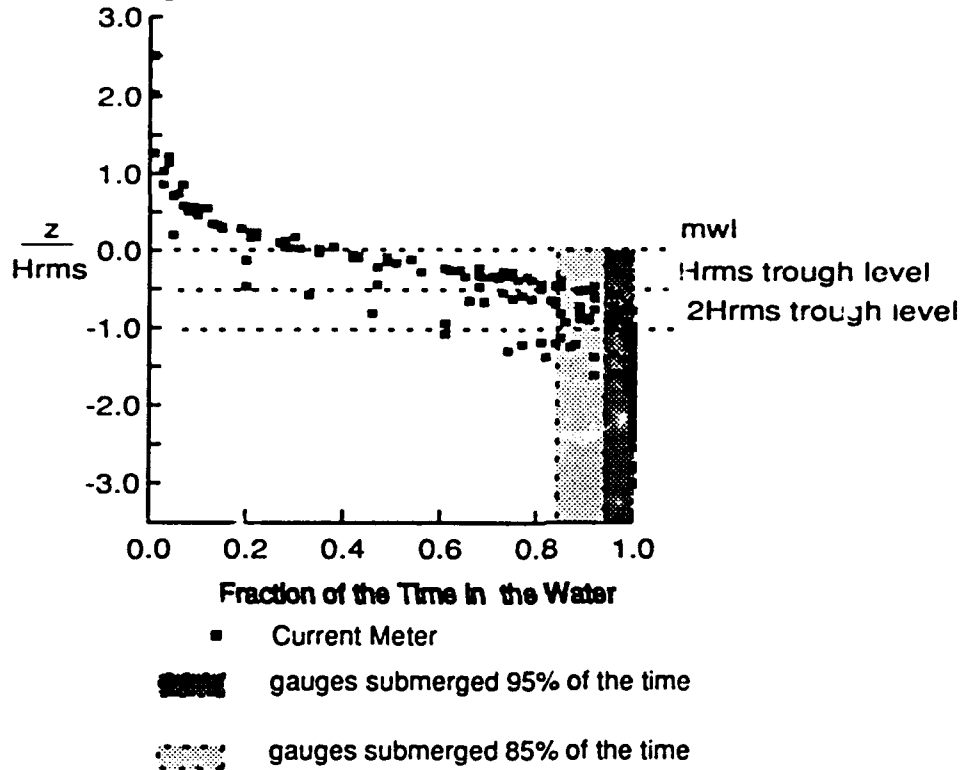


Figure 16: The location the Scripps current meters in relative water depth versus the fraction of the time they spent in the water.

Field Recalibration of the Current Meters

Twenty-six 1-hour-series were determined to be "low flow" runs based on having measured low waves and, by averaging these means, a new in-situ calibration offset was determined for the two outer stacks. The inner-most stack was not corrected in this way because we did not

feel confident that the flow was truly zero there. Only the large signal series were used as the final Scripps means in this study which left twenty-six 1 hour means for use in the model-data comparisons.

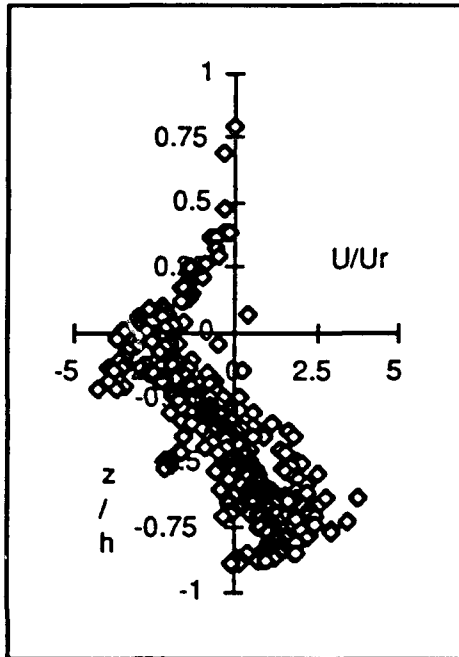


Figure 17: Scripps UnderTow data plotted on scaled axes. The mean current is scaled to U_r and the vertical axis is scaled to the water depth, h .

Model Data Comparisons

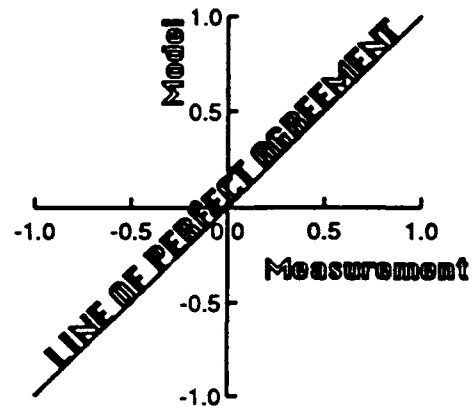


Figure 21: *The line of perfect agreement between the model and the measurements.*

How well do the models compare with the field data? What kinds of errors and correlations do we calculate? The answers to those questions depend on how and where we look. First we briefly examine the statistical methodology, how we implemented the model-data comparisons and what statistical measures we computed. Then, we discuss the models, starting with the simplest mass balance model. We identify "tunable" parameters and identify how they affect the statistical fit.

The Statistical Tests

The model data comparisons were accomplished by comparing the predicted values to their corresponding measured values. Lists of these comparisons, (Meas(i), Model(i)), were created by running the model against a subset of the field measurements.

Six statistical quantities are reported for each comparison. The linear regression statistics: slope, intercept and r-squared, are reported as a measure of scatter in the fit. Three quantities of error are reported, absolute error and two measure of relative error. Absolute error, computed using equation 49, has real units and is an rms measure of the difference between the model and the measurements. Relative error weights the difference between the model and the measurements against a measure of expectation. In this study we scale by the measurement, which we presume is accurate, and compute the relative error using equation 50. This statistic is not well-behaved near zero and we compensate by reporting two relative error statistics, first excluding measurement less than the reported accuracy of the current meters of +/- 3 cm/sec, (Guza et all, 1981) and second excluding measurements less than +/- 15 cm/sec. This last cutoff is arbitrary but gives us a feel for the relative error for the fit with all reasonable measurements in the entire data set and with a set restricted to large-ish mean currents which are presumably of interest.

$$\text{absolute error} = \sqrt{\frac{\sum_{i=1}^N (P_i - M_i)^2}{N}} \quad (49)$$

$$\text{percent error} = 100 \left[\sqrt{\frac{\sum_{i=1}^N \left(\frac{P_i - M_i}{M_i} \right)^2}{N}} \right] \quad (50)$$

A perfect match has all measures of error equal to zero, a slope of one, an intercept of zero and a correlation coefficient r-squared equal to zero. In practice the measures are far from perfect. A question we want to answer is, "Can we deduce the best fit from some combination of these statistical measures?"

The following designators will be used in reference to the statistical quantities:

absolute error: units are meters per second and values represents the rms distance between the measurements and the ideal case

percent error 1: relative error using only measurements outside the +/-3 centimeter per second threshold.

percent error 2: relative error using only measurements outside the +/-15 centimeter per second threshold.

r-squared: correlation coefficient squared

slope: slope of best fit line

intercept: intercept of best fit line

Mass Model - Scripps Data Comparisons

The mathematical definition of the mass model is given by equations 15 through 18. There are two parameters in the model we must set: the exponent n and the coefficient of saturation, γ . These variables control the amount of wave-breaking in the model. Maximum breaking occurs for small n and small γ , with the requirement that the weighting function $W(H)$, must be less than 1. Larger values predict that more than 100% of the waves are breaking. For a given γ , a large n predicts less breaking than a small n .

We chose a reasonable range of parameters: $n = 4, 5, 6$ and $\gamma = 0.4, 0.5, 0.6$, ran the model against the Scripps data and found that the model is generally insensitive to these choices for n and γ . The statistical results are plotted in Figure 18 from which we conclude that the mass model appears to be insensitive to the parameters n and γ .

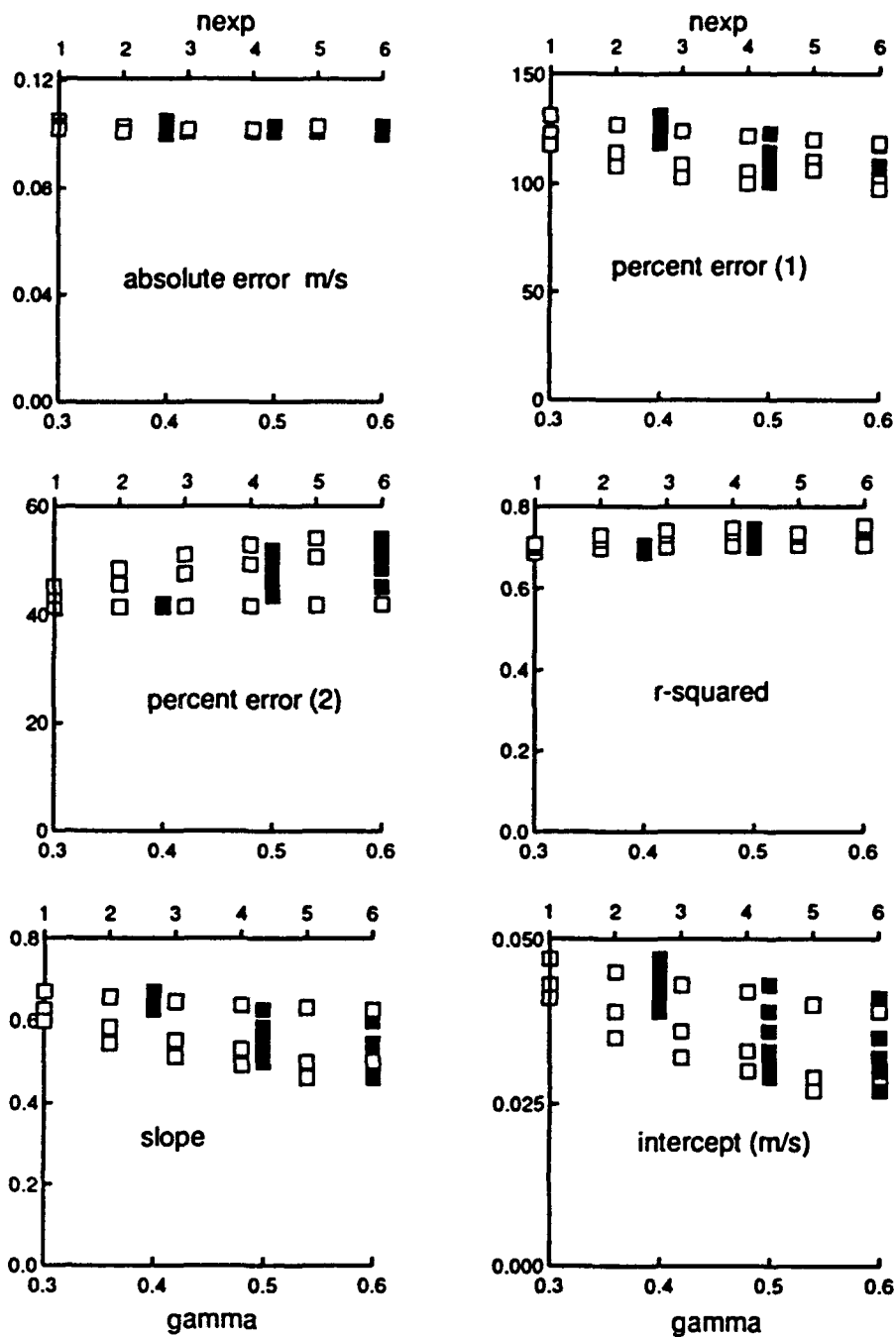


Figure 18: The statistical measures of fit between the mass model and the Scripps UnderTow data, graphed as a function of the parameters n and γ . The open boxes show the n_{exp} dependence, the solid boxes the γ dependence.

Scatter plots of the results using the two extreme (n , γ) pairs are shown in Figure 19. Points found in the first and third quadrants represent comparisons in which the model and the measurement were of the same sign. Positive values in the first quadrant represent off-shore flow while negative values in the third quadrant represent shoreward flow. Overall, the values predicted for the case with much wave breaking, ($n = 1$, $\gamma = 0.4$), are larger by a factor of approximately 1.3 times compared with a case with the little breaking, ($n = 6$, $\gamma = 0.6$). With maximum wave breaking there is more scatter and the relative error is larger than with minimal breaking.

The statistical measures for these two cases are listed in Table 3. The case with the minimal breaking has better overall numbers. The relative error, for measurements with a magnitude larger than 3 cm/s is 98% while for measurement with magnitude larger than 15 cm/s is 58%.

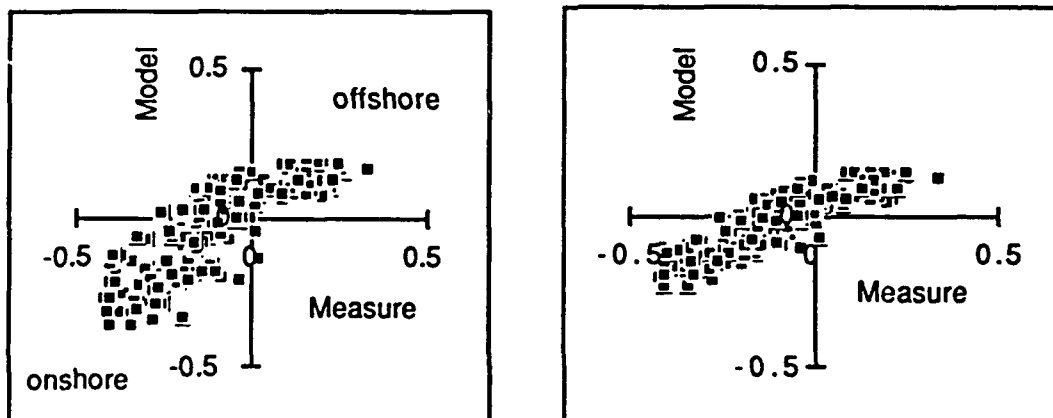


Figure 19: Scatter plots of the mass-model compared with all Scripps sensors. On the left is Case1 with parameters $n = 1$, $\gamma = 0.4$. On the right is Case2 with $n = 6$, $\gamma = 0.6$.

Statistical Measure	n=1; gamma=0.4	n=6; gamma=0.6
absolute error m/s	0.11	0.10
percent error 1 (3 cm/s)	132	98
percent error 2 (15 cm/s)	50	58
slope	0.66	0.47
intercept m/s	0.05	0.03
r-squared	0.68	0.75

Table 3: Statistical measures of fit for the mass model-data comparisons of the Scripps UnderTow data. Two pairs of parameters are tested.

Case 1 is with $n = 1$ and $\gamma = 0.4$. Case 2 is with $n = 6$ and $\gamma = 0.6$.

The next question we want to answer is, "How well does the mass model predict values below the wave trough level?" For the Scripps data we identified the meters below the trough level as meters which were submerged at least 95% of the time. A representative scatter plot and the statistical results are given in Figure 20:

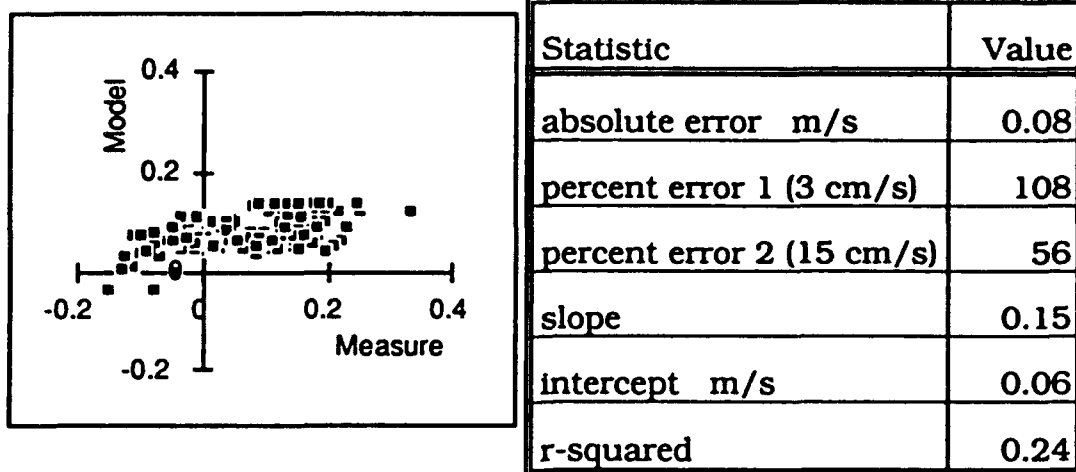


Figure 20: Scatter plots of the mass-model compared with the Scripps meters located below the wave trough. Model was run with $n = 6$, $\gamma = 0.6$.

All of the statistical estimates worsened except the absolute error which did not change significantly. Only the correlation statistics dropped dramatically. Visually, the fit worsened or at least fell farther from our ideal case.

Momentum Model - Scripps Data Comparisons

The momentum model is defined by equation 33 or 44. In this study we assume the bottom boundary layer is thin and model using equation 33.

The momentum model has the same parameters, n and γ , as the mass model though they are hidden in the wave forcing term, $dRdx$. B is an additional parameter used in modeling the wave height. We can confidently discharge the question "How well do we model the wave heights across the surfzone?" and show that the model is insensitive to reasonable values of n , γ and B .

The parameter B tunes the amount of energy dissipation in equation 47. The best B is one which minimizes the rms error between the predicted wave height and the measured. In our implementation we found a reasonable value of B for any (n, γ) pair. Figure 21 shows a typical scatter plot of the wave height fit.

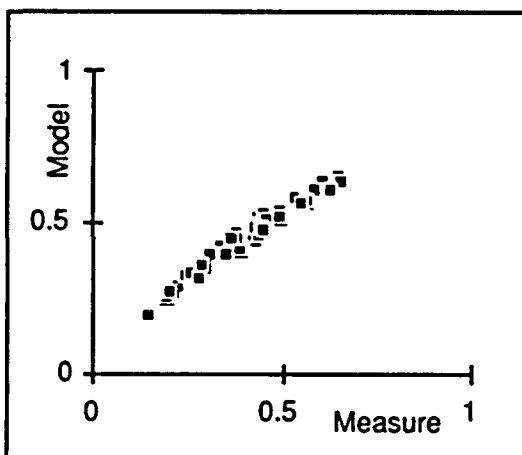


Figure 21: Scatter plot of the fit between the wave height predictions, and the Scripps measured wave heights. The results are with $n = 6$, $\gamma = 0.6$ and $B = 1.95$. The absolute error of the fit was 5 cm. The units on the graph are m/s.

This is a decent job of modeling the wave heights and we conclude that, if we're modeling H_{rms} accurately, we must be doing a reasonably good job of modeling its cross-shore gradient. Can we conclude that our model for dR/dx will be equally insensitive to our choices of tunable parameters?

We have no measure of dR/dx and must rely on mathematical intuition. Inside the surfzone dR/dx depends primarily on the gradient of the wave setup which, using linear theory, depends on the gradient of the radiation stress S_{xx} . Inside the surfzone $S_{xx} = 3E/2$, where E , the energy stored in a linear wave, is proportional to the wave height squared. Therefore, we conclude that the model for dR/dx is equally insensitive to our choice of n and γ .

The Eddy Viscosity Coefficient, ν_t

The eddy viscosity coefficient, ν_t has a marked affect on the amount of shear in the profile. Small ν_t makes for large shear while with large ν_t the profiles become effectively shearless. Stive and Wind, (1986), report a value of $\nu_t = 0.01 Ch$, taken from channel theory. We examined the behavior of the model a function of the scaling coefficient, ν_t where, $\nu_t = \nu_t^* Ch$ and found it to be quite predictable

We selected a liberal range of values to survey, varying ν from 0.0001 to 10. For small values we found, as predicted, that the shear in the profile is unrealistically large while for large ν , the limiting case is the straight profile predicted by the mass model. Figure 7 is a good example of this.

For a given value of ν , the shape of the profile is sensitive to the value of dR/dx . How will this vary across the surfzone? Wave setup, is effectively zero outside the surfzone and dR/dx is minimal, due only to changes in the wave orbital momentum. In a saturated surfzone the cross-shore gradient of the setup is maximum and approaches a constant, Guza and Thornton (1981). Figure 22 illustrates the model prediction at the three Scripps stacks for a particular run.

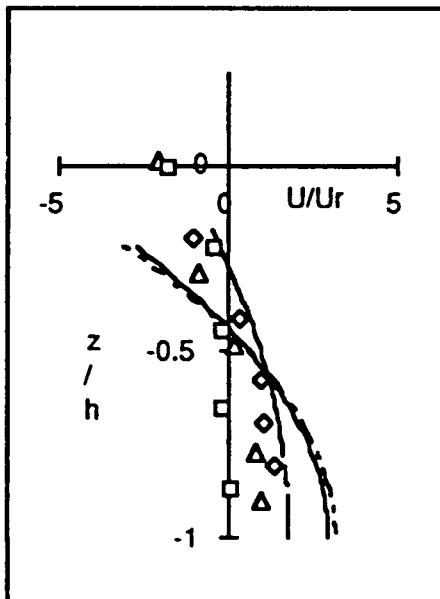


Figure 22: Typical scaled profiles predicted by of the momentum model. using $n = 1$, $\gamma = 0.4$ and $\nu = 0.001$, the model was run with against Scripps run 17ab. The predictions are the lines: solid represents the A-stack, dotted line the B-stack, and the dashed line the C-stack. The markers are measurements: diamonds represent the A-stack, triangles the B-stack and squares the C-stack.

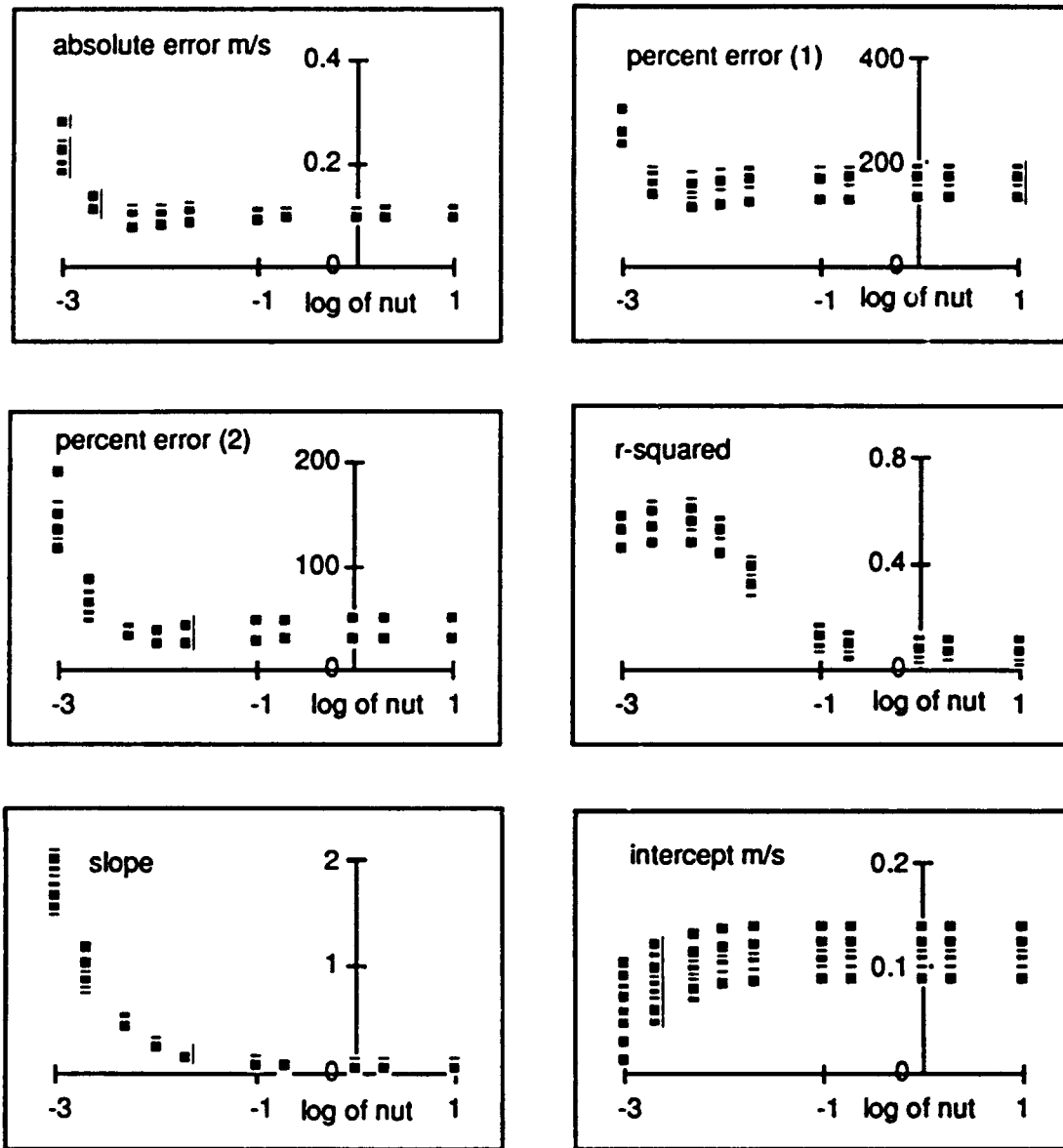


Figure 23: Statistical measures of fit between the momentum model and all Scripps data located below the wave trough.

Figure 23 gives a graphical representation of the variability of the fit as a function of nut. This confirms that the errors are large for unrealistically small values of nut and that for large values the momentum model predicts the simple mass results. The "best fit" was for nut = 0.002, n = 6 and gamma = 0.6. Except for a slight deviation in the r-squared all measures of fit were "best" for these parameters. A sample scatter plot and statistics are included in Figure 24

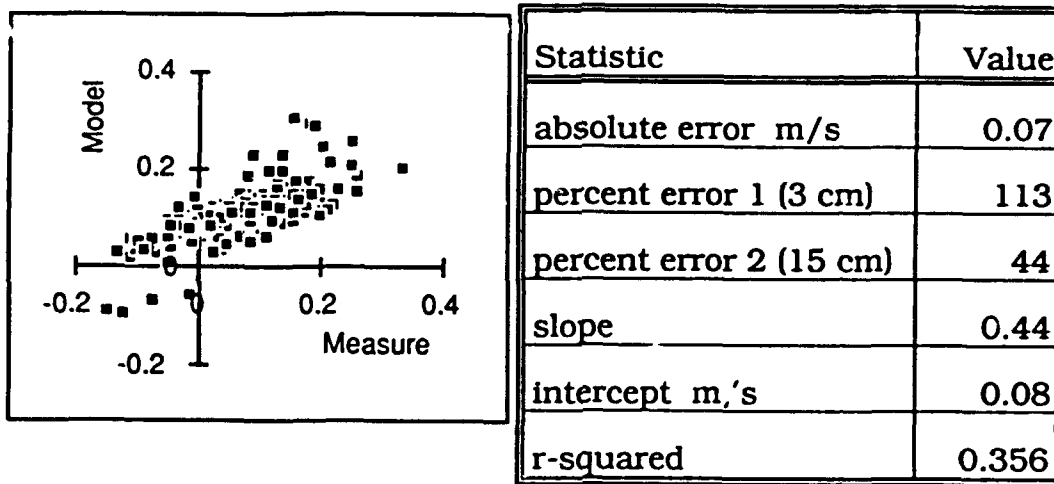


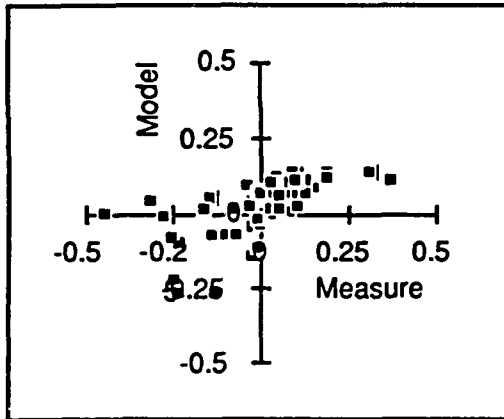
Figure 24: Scatter plot and statistics of the momentum model comparison with the Scripps data below trough level. Model was run with n = 6, gamma = 0.6 and nut = 0.002.

Can we conclude that this is a good or a bad fit? We should postpone this question until the final analysis. This may give us time to think of an alibi.

SuperDuck Comparisons

The SuperDuck comparisons can proceed directly since, by now, we should have a better feel for the model. We showed that the sensitivity to n and γ was minimal and we chose standard values of $n = 4$ and $\gamma = 0.42$ for this comparison. As before, we look first at the fit with the mass model before tackling the momentum model.

Mass Model Comparisons



Statistic	Value
absolute error m/s	0.11
percent error 1 (3 cm)	94
percent error 1 (15 cm)	70
slope	0.42
intercept m/s	0.03
r-squared	0.41

Figure 25: Scatter plot and table of statistics from comparison between the mass model with the SuperDuck data. Parameters were $n = 4$ and $\gamma = 0.42$.

Figure 25 illustrates the results of exercising the model with our choice of parameters with all of the SuperDuck dataset. It reveals a good deal of scatter in the fit, especially in the match with the negative onshore flows. The absolute error is 0.11 m, identical with the comparable Scripps results. The relative error is 135 percent which is smaller than by a factor of 2.4 times smaller than the comparable Scripps results. The correlation statistics are poorer for the Duck comparison due to the scatter we mentioned earlier. Would you say this is a better or a worse fit?

How well does the data from below trough level compare with the mass model? The scatter plot and statistics are found in Figure 26

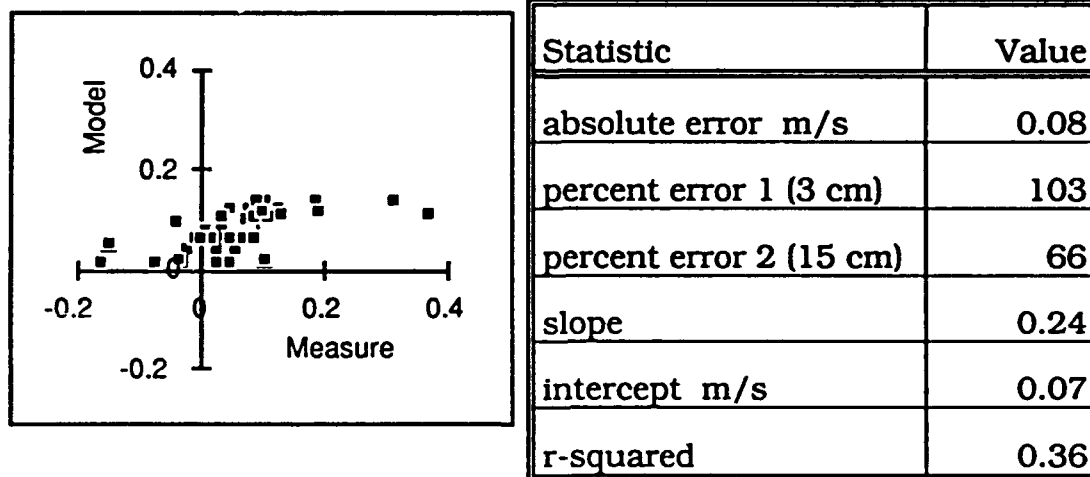


Figure 26 Scatter plot and statistics from the comparison between the mass model and the SuperDuck data located below the trough level using $n=4$ and $\gamma = 0.42$.

The errors are nearly the same as those found using the entire data set, but the correlation has dropped. This comparison with Duck data produced similar statistics values as did the Scripps comparisons.

Momentum Model Comparisons

The momentum model was exercised with the SuperDuck data located below the 2Hrms trough for fixed $n=4$ and $\gamma = 0.42$ and with a "reasonable" nut value of 0.002 .

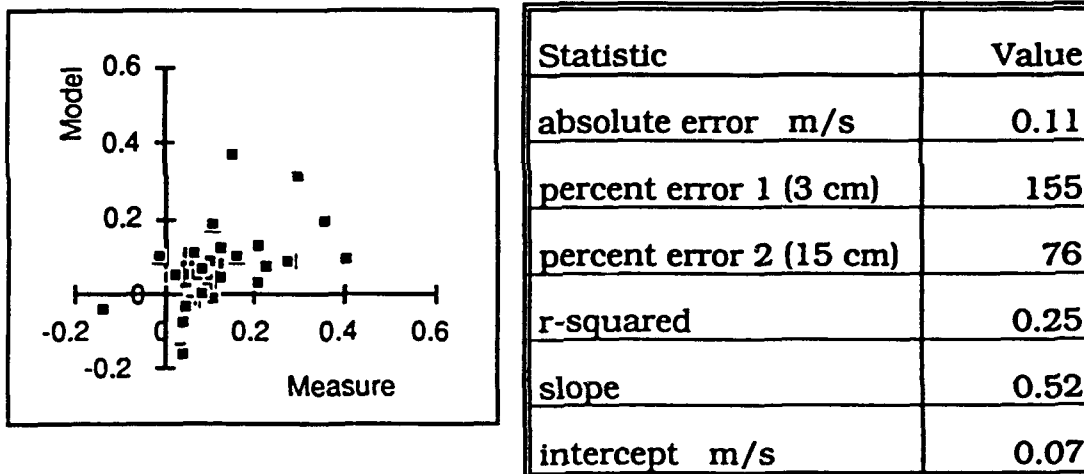


Figure 27: Scatter plot and statistics from the comparison between the momentum model and SuperDuck measurements located below the trough level. Values are computed using $\text{nut} = 0.002$.

Mean Currents Near the Sea Floor

We are finally prepared to ask a serious question. How well does the momentum model work when predicting "near bottom flow". For the purpose of this experiment, we will restrict ourselves to the lower quarter of the water column. At SuperDuck, the lowest current meter was at 0.7 meters above the bed and only 3 current meters fit this criteria. The Scripps data provides 49 suitable points. The results for the statistical fit are given in Figure 28.

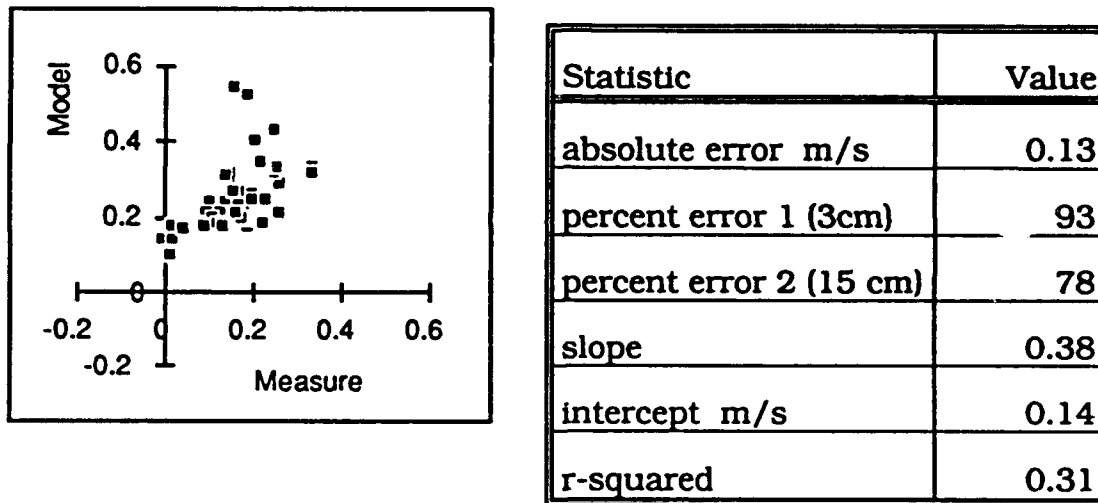


Figure 28: Scatter plot and statistics from the comparison between the momentum model and the Scripps sensors located in the lower quarter of the water column. Model was run using $n = 6$, $\gamma = 0.6$ and $\text{nut} = 0.002$.

Discussion

"Increasingly, the mathematics will demand the courage to face its implications" *Ian Malcom*

The Statistical Measures

Did our statistical measures prove to be meaningful? Can we find a single measure to use as a fitness test? The answer at this stage is no. The absolute error seems a good choice for parameterizing the range of the errors. Beyond that, it gives little additional information. The relative errors proved to be more sensitive to the change in parameters and, while they follow the same trend as the absolute error, the reported values are quite high. Is this because the errors were large or is this a figment of the scaling parameter we chose? We scaled the error by the measurement which we presume is correct. Is there a better choice? Apparently not.

The linear regression statistics, taken as a whole, are useful for observing the scatter of the comparison. The slope and intercept of the best fit line is an intuitive measure of fit. The slope can be used as a measure of how much the best fit line deviates from perfect. Taken alone, the correlation is not a good measure of fit.

The Mass Model

How well did the mass model compare with the field measurements? We found that the model was insensitive to the parameters n and γ which affect the predicted amount of wave breaking. The best results were obtained with the least breaking, $n = 6$ and $\gamma = 0.6$, but this still led to an under prediction of the measured values. The best-fit statistics for the mass model compared with the two data sets and their subsets are summarized in Table 4.

Data Set	absolute error m/s	percent error 1	percent error 2	r2	slope	intercept m/s	n	gamma
Scripps all sensors	0.10	98	58	0.75	0.47	0.03	6	0.6
Scripps sensors below trough	0.08	108	56	0.24	0.15	0.06	6	0.6
SuperDuck all sensors	0.11	94	70	0.41	0.42	0.03	4	0.42
SuperDuck below trough	0.08	103	66	0.36	0.24	0.07	4	0.42

Table 4: Summary of the statistical results of the comparison between the mass model and the field data used in this study

Momentum Model Comparisons

The behavior of the momentum model as a function of the eddy viscosity coefficient was well predicted by theory. Large errors were reported for small values of ν and, for large ν , the values converged to the mass-model results. A summary of the statistics for both data sets is reported in Table 5

Data Set	absolute error m/s	percent error 1	percent error 2	r2	slope	intercept m/s	n	gamma	nut
Scripps - below trough	0.07	113	44	0.36	0.44	0.08	6	0.6	0.002
SuperDuck - below trough	0.11	155	76	0.25	0.52	0.07	4	0.42	0.002

Table 5: Summary of best fit statistics for the comparison between the momentum model and the field data used in this study

Mean Currents Near the Bed

We ran the momentum model with the Scripps data located in the lowest quarter of the water column to determine how accurately we can predict the mean near-bottom currents. The results using parameter choices, $n = 6$, $\gamma = 0.6$ and $\nu = 0.002$ are summarized in Table 6.

Data Set	absolute error m/s	percent error 1	percent error 2	r2	slope	intercept m/s	n	gamma
Scripps sensors lower quarter	0.13	93	78	0.31	0.38	0.14	6	0.6

Table 6 Summary of the statistical results of the comparison between the mass model and the field data used in this study

Can we draw some conclusions from the results? The statistical values numbers do not vary much from data-set to data-set nor much from model to model. This is not a good sign. Overall, the mass model seems to do as good a job as the momentum model. The general shape of the profile is better described by the later, but the results based on our two sets of measurements can not distinguish between the two models.

What are some of the reasons for this? One question we can not answer is how well did the assumption of conservation of mass flux hold in these data sets? Using only 3 to 5 current meters in the vertical will give us only a rough quantitative measure of the mass flux. If water were

being lost or gained from the alongshore direction, the mathematics says the model will not work.

Another reason lies in the shear terms found in the momentum model which distribute the mass flux about the vertical line positioned at U_r . Thus, while we may be able to better predict the velocities in one part of the water column by injecting more or less shear into the model, the comparison with values elsewhere may suffer.

What kinds of future studies might resolve the open questions? Mathematical studies of the kind leading to improvements for the momentum model would be fruitful. Measurements which allow us to test how well we're modeling the wave forcing term seem invaluable. Perhaps with the new sonar technologies being developed we will be able to measure three components of velocity over a nearly continuous depth profile. More studies of wave setup and its cross-shore gradient will help quantify other important parameter of the model.

References

Ballard, J.A., and D.L. Inmann, An energetics bedload transport model for a plane sloping beach; local transport, *Journal of Geophysical Research*, vol. 86, C3, 2035-2043, 1981

Dally, W.R., and R.G. Dean, Mass Flux and Undertow in a SurfZone by I.A. Svendsen - Discussion, *Coastal Engineering*, 10, 289-307, 1986

Diegard, R., P. Justesen, J. Fredsoe, Modeling of Undertow by a One-Equation Turbulence Model, *Coastal Engineering* 15, 431-358, 1991

Fredsoe, J., and R. Deigaard, *Mchanics of Coastal Sediment Transport*, World Scientific Publishing Company, 1992

Greenwood, B., and P. Osborne, Vertical and Horizontal Structure in Cross-Shore flows: An Example of Undertow and Wave Set-Up on a Barred Beach, *Coastal Engineering*, 14, 543-580, 1990

Guza, R.T., and E.B. Thornton, Wave Set-Up on a Natural Beach, *Journal of Geophysical. Research* 86, C5, 4133-4137, 1981

Guza, R.T., M. C. Clifton, and F. Rezvani, Field Intercomparisons of Electromagnetic Current Meters, *Journal of Geophysical. Research* 93, C8, 9302-9314, 1988

Hwang, L.S. and D. Divoky, Breaking Wave Set-up and Decay on gentle Slopes, Proceedings of the 12th International Conference Coastal Engineering, American Society of Engineer, New York pp 377-389, 1970

Longuet Higgins, M. S., The Mechanics of the boundary-layer near the bottom in a progressive wave, Coastal Engineering, Proceedings of the International Coastal Engineering Conference, 184-193, 1956

Okayasu, A., T. Shibayama, and K. Horikawa, Vertical Variation of Undertow in the Surf Zone, Coastal Engineering, Proceedings of the International Coastal Engineering Conference, 479-490, 1988

Phillips, O. M., The Dynamics of the Upper Ocean, Cambridge University Press, Cambridge, 1977

Roelvink, J. A. and M. J. F. Stive, Bar-Generating Cross-Shore Flow Mechanisms on a Beach, Journal of Geophysical Research, 94, C4, 4785-4800, 1991

Russell, R. C. H. and J. D. C. Osorio, J.D.C.,
An Experimental Investigation of Drift Profiles in a Closed Channel,
Coastal Engineering, Proceedings of the International, Coastal
Engineering Conference, 171-183, 1956

Stive, M. J. F. and H. G. Wind, A study of radiation stress and set-up in the nearshore region, Coastal Engineering, 8:347-365, 1982

Stive, M. J. F. and H. G. Wind, Mean Cross-Shore Currents in the SurfZone, Coastal Engineering, 8:347-365, 1986

Stive, M. J. F. and H. J. de Vriend, Quasi-3D Nearshore Current Modelling: Wave-Induced Secondary Current, Coastal Hydrodynamics, Proceedings of a Conference of the American Society of Civilian Engineers., 356-370, 1987

Stoker, J. J., Water Waves, Interscience, New York, 1957

Svendsen, I. and B. Hansen, A Theoretical and Experimental Study of Undertow, Coastal Engineering, International Coastal Engineering Conference Proceedings, 2246-2262, 1984

Svendsen, I. H. Schaffer, and B. Hansen, The Interaction Between the Undertow and the boundary Layer Flow on a Beach, Journal of Geophysical Research, Vol. 92, No C11, 11,845-11,586, 1987

Svendsen, I. and B. Hansen, Cross-shore Currents in Surf-Zone Modelling, Coastal Engineering, 12 1988 23-42, 1988

Svendsen, I. and R. Lorenz, Velocities in Combined Undertow and Longshore Currents, Coastal Engineering, 13 1989 55-79, 1989

Thornton, E.B., Energetics of Breaking Waves Within the Surf Zone, Journal of Geophysical Research, 84, 18, 4931-4938, 1979

Thornton, E.B., and R.T. Guza, Transformation of Wave Height Distribution, Journal of Geophysical Research, 88, C10, 5925-5938, 1983

Uday, P. and I. Svendsen, Vertical Structure of the Undertow Outside the Surf-Zone, (in press)

Whitford, D. and E.B. Thornton E.B., Longshore Currents over a Barred Beach, I: Field Experiment, submitted to the Journal of Physical Oceanography, (in press)